Since January 2020 Elsevier has created a COVID-19 resource centre with free information in English and Mandarin on the novel coronavirus COVID-19. The COVID-19 resource centre is hosted on Elsevier Connect, the company's public news and information website.

Infectious Medicine 1 (2022) 7–16

Contents lists available at ScienceDirect

Infectious Medicine

journal homepage: www.elsevier.com/locate/imj

Original article

SARS-CoV-2 helicase NSP13 hijacks the host protein EWSR1 to promote viral replication by enhancing RNA unwinding activity

Hongxiang Zeng[a,#], Xiang Gao[a,#], Gang Xu[a,#], Shengyuan Zhang[a], Lin Cheng[a], Tongyang Xiao[a], Wenhong Zu[a], Zheng Zhang[a,b,c,*]

[a] Institute for Hepatology, National Clinical Research Center for Infectious Disease, Shenzhen Third People's Hospital, the Second Affiliated Hospital, School of Medicine, Southern University of Science and Technology, Shenzhen, Guangdong Province, China
[b] Shenzhen Research Center for Communicable Disease Diagnosis and Treatment of Chinese Academy of Medical Science, Shenzhen, Guangdong Province, China
[c] Guangdong Key Laboratory for Anti-Infection Drug Quality Evaluation, Shenzhe, Guangdong Province, China

ARTICLE INFO

Keywords:
Nsp13
Ewsr1
Unwinding

ABSTRACT

Background: Severe acute respiratory syndrome coronavirus 2 (SARS-CoV-2) emerged in December 2019 and has led to a global coronavirus disease 2019 (COVID-19) pandemic. Currently, incomplete understanding of how SARS-CoV-2 arrogates the host cell to establish its life cycle has led to slow progress in the development of effective drugs.

Results: In this study, we found that SARS-CoV-2 hijacks the host protein EWSR1 (Ewing Sarcoma breakpoint region 1/EWS RNA binding protein 1) to promote the activity of its helicase NSP13 to facilitate viral propagation. NSP13 is highly conserved among coronaviruses and is crucial for virus replication, providing chemical energy to unwind viral RNA replication intermediates. Treatment with different SARS-CoV-2 NSP13 inhibitors in multiple cell lines infected with SARS-CoV-2 effectively suppressed SARS-CoV-2 infection. Using affinity-purification mass spectrometry, the RNA binding protein EWSR1 was then identified as a potent host factor that physically associated with NSP13. Furthermore, silencing EWSR1 dramatically reduced virus replication at both viral RNA and protein levels. Mechanistically, EWSR1 was found to bind to the NTPase domain of NSP13 and potentially enhance its dsRNA unwinding ability.

Conclusions: Our results pinpoint EWSR1 as a novel host factor for NSP13 that could potentially be used for drug repurposing as a therapeutic target for COVID-19.

1. Introduction

Severe acute respiratory syndrome coronavirus 2 (SARS-CoV-2) is responsible for the coronavirus disease 2019 (COVID-19) outbreak that has caused over 364 million infections, resulting in a serious global pandemic since December 2019 [1–5]. Currently, there is an urgent need to better understand the molecular mechanisms of SARS-CoV-2 replication because this information will provide vital insights for the design of better drugs and vaccines. SARS-CoV-2 belongs to a large family of single-stranded, positive-sense RNA viruses containing large RNA genomes of 26–31 kb, and encoding 2 large open reading frames (ORFs) called ORF1a and ORF1b [6]. These ORFs are translated into 2 polyproteins, pp1a and pp1ab, which are proteolytically cleaved into the 4 structural proteins, spike (S), envelope (E), membrane (M), and nucleocapsid (N) proteins, along with 16 nonstructural proteins (NSP1–16) and several accessory proteins named by ORF, which have been reported to modulate

Abbreviations: SARS-CoV-2, severe acute respiratory syndrome coronavirus 2; COVID-19, coronavirus disease 2019; NSP13, nonstructural protein 13; EWSR1, Ewing Sarcoma breakpoint region 1/EWS RNA binding protein 1; TAD, transcriptional activating domain; RRM, RNA recognition motif; RBD, RNA binding domain; NP, nucleocapsid protein; RdRP, RNA-dependent RNA polymerase.

* Corresponding author.
E-mail address: zhangzheng1975@aliyun.com (Z. Zhang).
# These authors contributed equally: Hongxiang Zeng, Xiang Gao, and Gang Xu.

https://doi.org/10.1016/j.imj.2021.12.004
Received 25 October 2021; Received in revised form 11 December 2021; Accepted 29 December 2021

host immune responses [7–10]. NSP12 and NSP13 reside in the functional center for virus replication: NSP12 is an RNA-dependent RNA polymerase (RdRp) required for genome replication [11–13], while NSP13 possesses helicase activity for unwinding double stranded RNA (dsRNA) during the replication process [14–19].

Most RNA viruses, including coronaviruses (CoV-NL63, SARS-CoV, and Middle East respiratory syndrome coronavirus) and Flaviviridae (Zika virus and Dengue virus) produce dsRNA during viral replication, and so the RNA genome must be unwound for the next round of viral RNA replication to occur [20,21]. Therefore, the viral helicase responsible for this unwinding activity represents an important drug target for inhibiting viral replication. Ivermectin has been found to be a potent inhibitor of flavivirus replication, specifically targeting the NS3 helicase activity of the Kunjin virus (an Australian variant of West Nile virus) [22]. ASP2151, a helicase-primase inhibitor has been found to inhibit replication of thymidine kinase-deficient herpes simplex virus 2 [23]. A clinical trial of amenamevir has been completed and licensed successfully, holding great promise for treating herpes zoster [24]. Thus, we believe that there is important potential in exploring host dependencies of the SARS-CoV-2 helicase NSP13 to identify other host proteins that are already targeted by existing drugs.

EWSR1 (Ewing Sarcoma breakpoint region 1/EWS RNA binding protein 1) is ubiquitously expressed in most cell types and has many roles in distinct cellular processes and organ development [25–29]. EWSR1 has been reported to interact with heterogeneous RNA-binding proteins (hnRNPs), such as RBM38 and RBM39, which are involved in alternative RNA splicing [30]. It is noteworthy that EWSR1 protein can directly bind RNA in vitro, which is achieved by its C-terminal domain containing an RNA-recognition motif (RRM) and three RGG boxes [31]. It has been reported to interact with the cis-acting replication element (CRE) of hepatitis C virus, acting as a potential cofactor for virus replication [32]. A recent study also demonstrated that EWSR1 potentially binds to the SARS-CoV-2 genome directly [33]. However, it is not yet known whether EWSR1 regulates SARS-CoV-2 replication, or the specific mechanism by which this may occur.

In the current study, using mass spectrometry, we identified EWSR1 as a potent binding partner of SARS-CoV-2 helicase NSP13. Domain-mapping analyses revealed that the NTPase domain of NSP13 associates with the RNA binding domain (RBD) of EWSR1. Knockdown of EWSR1 can efficiently block SARS-CoV-2 replication, while supplementing the expression of EWSR1 can rescue viral replication. Finally, an in vitro dsRNA unwinding assay revealed that EWSR1 promotes the unwinding ability of NSP13. Thus, our findings identify a novel host factor for SARS-CoV-2 replication that could potentially be targeted for therapy.

2. Materials and methods

2.1. Construction of expression vectors

For the eukaryotic expression vectors, the pcDNA6B-NSP13-flag plasmid was kindly provided by Prof. Peihui Wang from Shandong University, and the CMV-EWSR1-myc expression vector was purchased from Sino Biological Inc.

The NSP13 and EWSR1 truncations were constructed by designing truncation primers for PCR amplification (TransStart Fast Pfu DNA Polymerase, Transgene), followed by KpnI digestion of the original template plasmid at 37 ˚C for 2–4 h, then T4 polynucleotide kinase (TAKARA) mediated 5′ phosphorylation at 37 ˚C for 30 min and T4 DNA ligase (TAKARA) mediated ligation at room temperature for 1 h. GFP-tagged EWSR1 and mcherry-tagged NSP13 were constructed using a C113 ClonExpress MultiS One Step cloning kit (Vazyme).

For the prokaryotic expression vectors, the pET28a-6xHis-NSP13 plasmid was provided by Prof. Peihui Wang. The full-length human EWSR1 CDS was amplified from the CMV-EWSR1-myc template plasmid and cloned into the pET28a vector flanked by NdeI and XhoI. Truncated fragments TAD and RBD were generated by PCR from the full-length EWSR1 template and cloned into the pET28a vector.

2.2. Cell culture, transfection, cell lysis, and antibodies

HEK-293T, Huh7, and HeLa-ACE2 cell lines were cultured using DMEM supplemented with 10% fetal bovine serum (FBS) (Gibco) and 1% penicillin-streptomycin (Gibco). The Calu-3 cell line was cultured using alpha-MEM (Gibco) supplemented with non-essential amino acids, sodium pyruvate, and FBS (10%). The plasmids were adjusted to 3 μg for 6 well plates and 6 μg for 60 mm dishes, then mixed with polyethylenimine (PEI) (Sigma) transfection reagent in a 1μg:3μL ratio of plasmid:transfection reagent following the manufacturer's recommendations. After more than 30–36 h, cells were subsequently washed twice with PBS. Each step was performed by centrifugation at 600 × g, 4 ˚C for 5 min. Cell pellets were lysed with 2 × SDS sampling buffer and boiled at 95 ˚C for 15–30 min. Flag, c-myc, GAPDH, tublin, and actin antibodies were purchased from Transgene; EWSR1 antibody was purchased from Abcam; NP antibody was purchased from Sino Biological Inc; strep-tag II antibody was purchased from GenScript.

2.3. Virus infection, cellular, and supernatant viral RNA quantification and western blot

For the NSP13 inhibitor experiment, approximately 2 × 10^5 Huh7, VeroE6, Calu-3, and HeLa-ACE2 cells

were plated in 24 well plates, cultured with 10% FBS overnight and the next day were infected with SARS-CoV-2 (isolate Wuhan 2019) at a multiplicity of infection (MOI) of 0.2. One hour after infection, cells were washed thrice with PBS and media was replaced with 2% FBS full culture medium containing the indicated concentrations of inhibitors for 48 h postinfection. For RNA analysis, cells were collected at the indicated time and lysed in TRIzol. Total RNA was extracted according to the manufacturer's instructions. Supernatant was collected, heat inactivated at 95 ˚C for 5 min, and viral RNA was extracted using a viral RNA QIAamp viral RNA mini kit (QIAGEN). Reverse transcription quantitative (RT-q) PCR analysis was used to quantify viral RNA present in the supernatant and cells. NP gene primers 5′-TAATCAGACAAGGAACTGATTA-3′ (forward) and 5′-CGAAGGTGTGACTTCCATG-3′ (reverse) were used with the AceQ Universal SYBR qPCR master mix (Vazyme) in an Applied Biosystems QuantStudio 6 thermocycler. For protein analysis, whole cell lysates were obtained by lysing in 2 × SDS sampling buffer and proteins were separated by SDS-PAGE.

2.4. Flag tag affinity purification and mass spectrometry

To identify proteins associated with NSP13, HEK-293T, and HeLa cells plated in 15 cm dishes were transiently transfected with 15 μg pCMV-NSP13-flag plasmids using PEI. At 36 h post transfection, cells were washed twice with PBS, followed by lysing with 5 mL NP-40 lysis buffer containing 0.5% Nonidet P-40, 50 mM Tris (pH 7.5), 150 mM NaCl, 1 mM EDTA, 10% glycerol, protease inhibitor cocktail (Thermo Scientific), and phosphatase inhibitor (Thermo Fisher Scientific) at 4 ˚C for 30 min. Cell lysates were cleared by centrifugation at 12,000 g at 4 ˚C for 10 min. The supernatant was incubated with 5 μg flag antibody overnight, followed by addition of 200 μL protein G sepharose beads (Thermo Fisher Scientific) for another 3–4 h. The immunocomplex was washed twice with NP-40 lysis buffer and then three times with PBS with 0.1% Triton X-100. Associated proteins were eluted with 2 × SDS sampling buffer and boiled at 95 ˚C for 10 min. Proteins were loaded onto 10% SDS-PAGE and the gel was stained with Coomassie brilliant blue R-250 staining solution (Bio-Rad Laboratories) following the manufacturer's instructions. The heavy and light IgG bands were then excised, and the rest of the gel was sent to The PTM BioLab (Hangzhou, china) for mass spectrometry analysis.

2.5. Co-immunoprecipitation and immunoblot analysis

Cells were harvested at 36 h after plasmid transfection in 60 mm dish and washed twice with ice-cold PBS, then lysed in TNTE lysis buffer containing 20 mM Tris pH 7.5, 150 mM NaCl, 0.5% TritonX-100, 1 mM EDTA, 0.5% NP-40 supplemented with 1 mM PMSF and Protease Inhibitor Cocktail (100X) at 4 ˚C for 30 min. Cell lysates were cleared by centrifuging for 10 min. Then the supernatant was used for immunoprecipitation with 1 μg flag, myc or strep-tag II antibody overnight followed by addition of 20 μL protein G sepharose beads for another 3–4 h the next day. The beads were extensively washed with PBS with 0.1% TritonX-100 and eluted with 2 × SDS loading buffer by boiling at 95 ˚C for 5 min. For immunoblot analysis, the samples were separated by SDS-PAGE and transferred to a polyvinylidene fluoride (PVDF) membrane (Millipore). The membrane was incubated with the indicated primary antibody overnight and washed thrice in TBST buffer, followed by incubation of horseradish peroxidase-labelled secondary antibody for 1 h at room temperature. Proteins were visualized using an enhanced chemiluminescence detection system (Bio-Rad Laboratories).

2.6. Short haipin RNA (shRNA) construction, lentivirus packaging and RNA interference

shRNAs targeting the EWSR1 were selected using the RNAi Consortium (TRC) website from the Broad Institute. The shRNA oligonucleotides were synthesized by Sangon Biotech (Shanghai) Co. Ltd. We designed three shRNAs for human EWSR1 with the following sequences. shRNA-1, 5′-GCATTGACTACCAGATTTAT-3′; shRNA-2, 5′-ACAGCCTCCCACTGGTTATA-3′; shRNA-3, 5′-GCATTGACTACCAGATTTAT-3′. We chose the most effective shRNA-1 for the rescue experiment. The single strand RNA was annealed and inserted into the pLKO.1 lentiviral vector linearized by AgeI and EcoRI. For transduction of shRNA in the Huh7 cell line, lentiviruses expressing scramble and EWSR1 shRNA were produced by PEI transfection in HEK-293T cells (10 cm plate) containing 10 μg pLKO. 1-shRNA vector, 6 μg PSPAX2, and 3 μg PMD2G. The viral supernatant was collected 48 h and 72 h post-transfection. All lentiviral transductions were performed by addition of polybrene at a final concentration of 4 μg/mL. The cells were transduced for 2 days and selected with a final concentration of 2 μg/mL puromycin for 2–3 days. The knock-down efficiency was determined by western blot at 72 h after puromycin selection.

2.7. Bacterial expression and protein purification

For expression and purification of the recombinant N terminal 6xHis proteins, pET28a-6xHis-NSP13, and pET28a-6xHis-EWSR1 FL/TAD/RBD plasmids were transformed into BL21-DE3 cells overnight followed by growing in 1 L LB medium at 37 ˚C until absorbance A_{600}=0.7. Protein expression was then induced by the addition of 0.3 mM isopropyl-β-D-thiogalactoside, followed by incubating cells at 22 ˚C for 14 h. For the purification of 6xHis tagged proteins, cell pellets were centrifuged at 2,000 g at 4 ˚C for 10 min and re-suspended in binding buffer containing 20 mM Tris–HCl pH8.0, 500 mM NaCl, and 10 mM

imidazole, then lysed by high-pressure ultra-sonication. Cell lysates were centrifuged at 12,000 g for 15 min at 4 ˚C. Supernatants were incubated with pre-balanced nitrilotriacetic acid Sepharose beads (Transgene) in 4 ˚C for 1 h, then loaded on a purification column (QIAGEN), washed with washing buffer containing 20 mM Tris–HCl pH 8.0, 500 mM NaCl, and 20 mM imidazole, followed by eluting with the elution buffer containing 20 mM Tris–HCl pH 8.0, 500 mM NaCl, and 50–200 mM imidazole. The eluted proteins were loaded on Amicon Ultra-30 filters and condensed by centrifuging at 2,000 g at 4 ˚C for 1–3 h. Following this, the storage buffer was exchanged for 50 mM 2-[4-(2-hydroxyethyl)-1-piperazinyl] ethane sulfonic acid (HEPES)-KOH (pH7.5). Proteins were quantified by the Pierce™ BCA protein assay kit (Thermo fisher Scientific) and stored at −80 ˚C in aliquots. Proteins were separated by 10% SDS-PAGE and visualized by Coomassie blue staining.

2.8. Preparation of dsRNA helix substrate and dsRNA helix unwinding assay

The dsRNA helix substrates consisted of 2 complementary RNA strands. One was a 42-bp RNA strand labeled with hexachloro-fluorescein phosphoramidite (HEX), and the other non-labeled strand was 24-bp long. The HEX-labeled and unlabeled strands were both synthesized by Sangon Biotech (Shanghai) Co. Ltd. The sequences of the oligonucleotides are listed in Table S1.

The dsRNA with 5′-protrusions were generated by annealing the HEX-labeled and unlabeled strands in a 1:1 ratio in a 50 μL reaction mixture containing 25 mM HEPES-KOH (pH 7.5) and 25 mM NaCl, followed by heating to 95 ˚C and cooling down gradually to room temperature.

The standard dsRNA unwinding assay was performed as previously described. Briefly, the indicated concentration of recombinant protein and 0.2 pmol/L of HEX-labeled helix dsRNA was mixed to the standard reaction mix containing 50 mmol/L HEPES-KOH (pH 7.5), 50 mmol/L NaCl, 2.5 mM $MgCl_2$, 5 mM ATP, and 15 U RNasin (TAKARA). After incubation at 37 ˚C for 10–15 min, the reaction was stopped by adding 10 × loading buffer containing 50 mM Tris-HCl, 50% glycerol, and 0.1% bromophenol blue. The mixtures were separated on 15% TBE-based native-PAGE gel at an initial voltage of 150 V for 15 min, followed by 200 V for 30–40 min, and then were scanned with ChemiDoc Imaging Systems (Bio-Rad Laboratories) at a fluorescence channel of Alexa Fluor 568.

2.9. Statistical analysis

Data were analyzed using GraphPad Prism software version 8.0 (GraphPad software, San Diego, CA). All results were considered significant for p values <0.05.

3. Results

3.1. NSP13 helicase activity is essential for SARS-CoV-2 replication

Considering the high homology (99%) of NSP13 in SARS-like coronaviruses, we sought to explore whether we could inhibit SARS-CoV-2 replication by using SARS-CoV NSP13 inhibitors. We chose three inhibitors for the NSP13 inhibition assay. SSYA10-001 has been demonstrated to be a potent and non-competitive inhibitor for NSP13, inhibiting the unwinding activities of NSP13 while not affecting ATP hydrolysis or NSP13 binding to the nucleic acid substrate in the SARS-CoV life cycle [14]; scutellarein potently inhibits the SARS-CoV helicase protein in vitro by affecting the ATPase activity, but not the unwinding activity of NSP13 [34]; and bismuth salts could effectively inhibit both the NTPase and RNA helicase activities of SARS-CoV-2 NSP13 [35,36]. We then treated Huh-7, Vero, and Calu-3 cell lines, which endogenously express ACE2, and the HeLa-ACE2 cell line, which exogenously expresses ACE2, with the three inhibitors at the indicated concentrations during virus infection. We found that scutellarein could dramatically reduce nucleoprotein (NP) levels in a dose-dependent manner in Vero cells (Fig. 1A) while it effectively inhibited NP expression at 100 μmol/L in Huh-7 cells (Fig. 1A). Scutellarein also inhibited NP expression in a dose-dependent manner in HeLa-ACE2 cells but had only mild effects on Calu-3 cells (Fig. 1A). Bismuth inhibited NP levels in HeLa-ACE2 cells (Fig. 1B). In addition, SSYA10-001 also exhibited effective inhibition of NP expression in a dose-dependent manner in Huh-7 and Vero cells, but the effective concentration was 100 μmol/L in HeLa-ACE2 and Calu-3 cells (Fig. 1C).

These results indicate that the three inhibitors the inhibitors had similar effects against SARS-CoV and SARS-CoV-2 and therefore may be applicable for use in treating future coronavirus outbreaks; however, more preclinical/clinical studies are needed to confirm whether this is effective in the clinic.

3.2. EWSR1 was screened as a potent binding partner of NSP13

To explore the role of NSP13 in virus-host interactions, we used a flag-tagged affinity purification mass spectrometry approach to identify the human proteins that physically interacted with NSP13 in both 293T and HeLa cell lines. We also used NSP16 as a non-specific control to compare with the NSP13 interactome. Immunoprecipitated protein complexes were captured by flag antibody and protein A beads, washed, separated by sodium dodecyl-sulfate polyacrylamide gel electrophoresis (SDS-PAGE), and stained with Coomassie blue. The

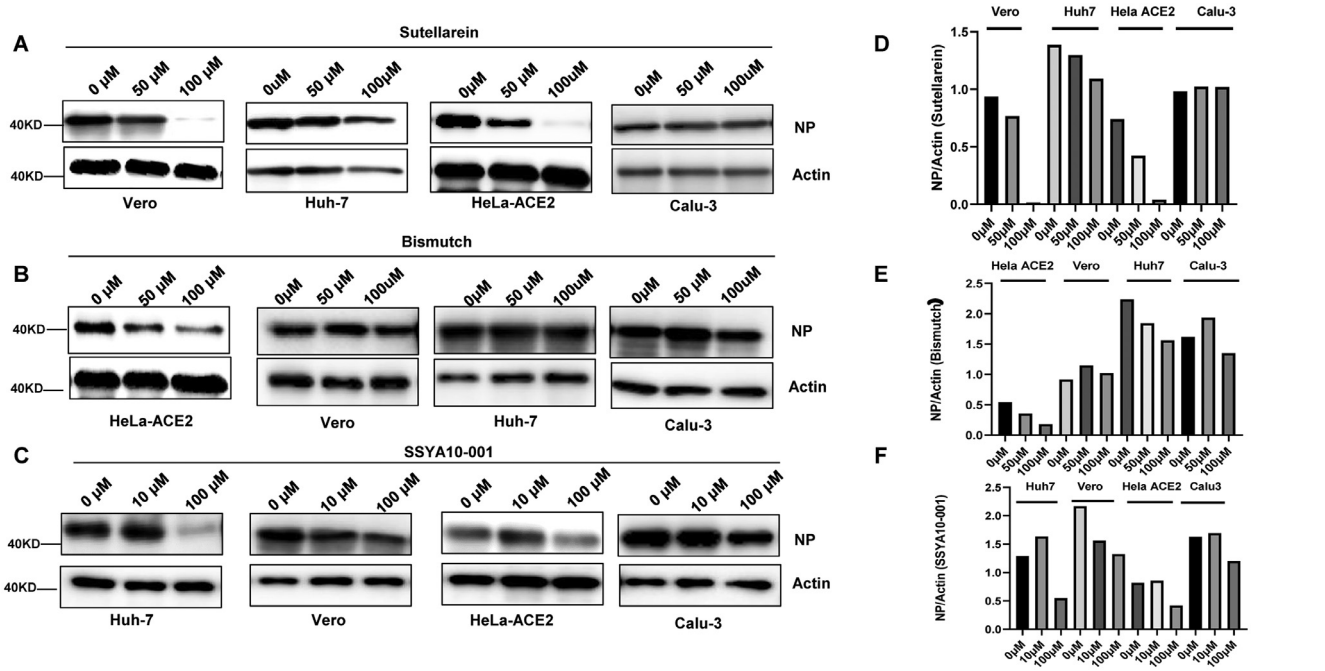

Fig. 1. SARS-CoV-2 helicase NSP13 is essential for viral replication. Huh-7, Vero, Calu-3, and HeLa-ACE2 cell lines were infected with SARS-CoV-2 at an MOI of 0.2 for 48 h. NSP13 inhibitors (A, scutellarein; B, bismuth; C, SSYA10-001) were subsequently added after viral infection and the respective concentrations are indicated. Viral NP protein expression was measured by western blot analysis. Quantified results are shown (D–F). (Color version of figure is available online.)

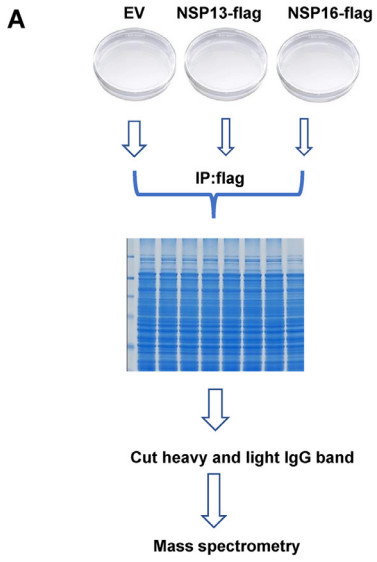

B

	Protein name	MS/MS count IP: flag vector	MS/MS count IP: NSP13-flag	MS/MS count IP: NSP16-flag
293T 1st	EWSR1	0	1	0
293T 2nd	EWSR1	0	1	0

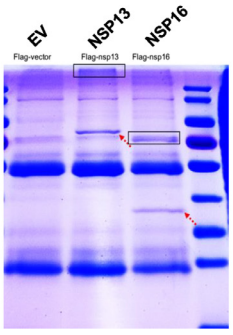

Fig. 2. Determination of the host factors associated with SARS-CoV-2 NSP13. (A) Schematic of the mass spectrometry analysis of NSP13 immunoprecipitates. Briefly, we overexpressed pCMV-NSP13-flag plasmid in 293T cells (empty vector and pCMV-NSP16-flag as control groups) followed by immunoprecipitation with flag antibody. Associated proteins were eluted with SDS buffer and then subjected to 10% SDS-PAGE. After Coomassie brilliant blue staining, IgG-heavy (52 kDa) and IgG-light (25 kDa) bands were excised, and the remaining gel was sent to The PTM BioLab (Hangzhou, china) for mass spectrometry analysis. Mass spectra were extracted, deconvolved, and deisotoped using Proteome Discoverer 1.4.1.14 (Thermo) and searched through the database (Homo sapiens, UniprotKB/Swissprot) for quantification analysis. (B) The number of EWSR1 peptides detected by mass spectrometry are shown in 2 separate experiments using HEK-293T cells. (C) Immunoprecipitates were subjected to SDS-PAGE and stained with Coomassie blue. Dotted arrows show immunoprecipitated NSP13 and NSP16. The bands in the closed boxes are specific binding partners of either NSP13 or NSP16.

heavy and light IgG bands were excised and the remainder of the gel was analyzed by matrix-assisted laser desorption ionization–mass spectrometry to identify the associating proteins (Fig. 2A). The dotted arrows show immunoprecipitated NSP13 and NSP16. The bands in the closed boxes are specific binding partners of either NSP13 or NSP16 (Fig. 2C). We identified several differential binding proteins including an RNA-binding protein called EWSR1. We found that EWSR1 was present in 2 distinct batches of experiments among all the identified interactions (Fig. 2B). To validate this interaction, we performed co-immunoprecipitation (co-

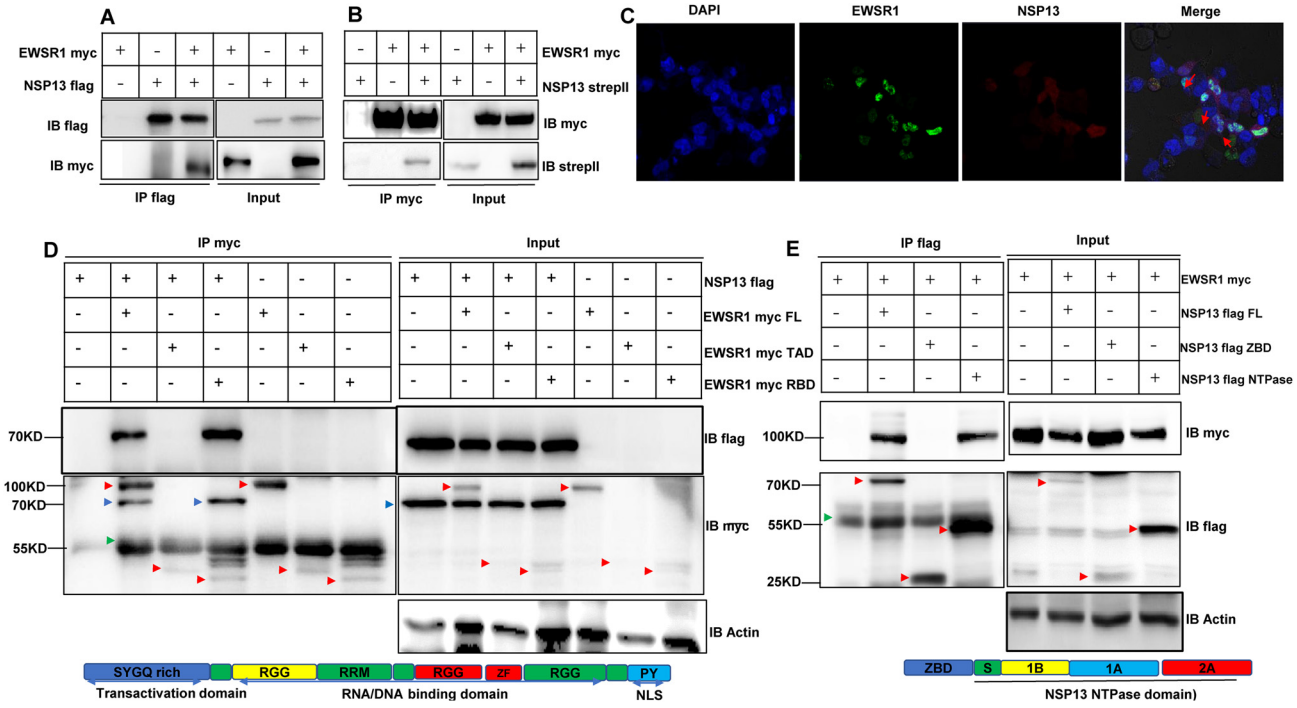

Fig 3. Domain mapping for the SARS-CoV-2 NSP13 and EWSR1. (A) HEK-293T cells were transiently co-transfected with NSP13-flag and EWSR1-myc plasmids for 36–40 h, followed by co-immunoprecipitation with flag antibody and immunoblot analysis with myc antibody. (B) HEK-293T cells were transiently co-transfected with NSP13-strepII and EWSR1-myc plasmids for 36–40 h, followed by co-immunoprecipitation with myc antibody and immunoblot analysis with the strep-tag II antibody. (C) 293T cells were transfected with GFP-EWSR1 and mcherry-NSP13 for 24 h. EWSR1 and NSP13 co-localization was analyzed by confocal microscopy. (D) HEK-293T cells were transiently co-transfected with NSP13-flag and plasmids expressing respective truncated EWSR1-myc fragments for 36–40 h, followed by immunoprecipitation and western blot. The functional EWSR1 domains are also shown below. (E) HEK-293T cells were transiently co-transfected with EWSR1-myc and plasmids expressing respective truncated NSP13-flag fragments for 36–40 h, followed by immunoprecipitation and western blot. The functional NSP13 domains are also shown below.

IP) assays and found that EWSR1-myc co-precipitated with NSP13-flag when pulled-down with flag antibody (Fig. 3A). Consistently, NSP13-strepII could be co-precipitated with EWSR1-myc when pulled-down with myc antibody (Fig. 3B). We also confirmed this interaction by performing an IP assay with endogenous EWSR1. EWSR1 co-precipitated with NSP13-flag when pulled-down with flag antibody (Fig. S1). Furthermore, green fluorescent protein (GFP)-EWSR1 was co-localized with mcherry-NSP13 in immunofluorescence analysis when co-expressed in 293T cells (Fig. 3C). It is noteworthy that there is no high quality commercially available NSP13 antibody to perform endogenous immunofluorescence during viral infection (data not shown).

EWSR1 contains an N-terminal serine-tyrosine-glycine-glutamine (SYGQ)-rich domain that acts as a transcriptional activating domain (TAD), an RRM, and a zinc finger domain involved in RNA and DNA binding, as well as multiple Arg-Gly-Gly (RRG)-rich regions in the C-terminus that affect RNA binding (the RNA binding domain, RBD), and a proline-tyrosine (PY) region that functions as a nuclear localization signal [37]. To further pinpoint the region of EWSR1 that is required for the interaction with NSP13, EWSR1 was truncated into its TAD and RBD domains. We found that only the RBD domain of EWSR1 co-precipitated with flag-tagged NSP13 and this interaction was comparable with that of the full length EWSR1 (Fig. 3D).

Conversely, to identify the region of NSP13 that is essential for the interaction with EWSR1, we truncated NSP13 into the N-terminal zinc binding domain (ZBD) and C-terminal NTP/ATP hydrolysis-dependent unwinding activity domain (NTPase domain) [38]. We found that only the NTPase domain of NSP13 co-precipitated with myc-tagged EWSR1 and this interaction was comparable with that of the full length NSP13 (Fig. 3E), suggesting that EWSR1 may promote virus replication by associating and enhancing the ATP hydrolysis process, thus promoting NSP13-mediated unwinding of dsRNA.

3.3. *EWSR1 is essential for SARS-CoV-2 replication*

To further determine the biological role of EWSR1 in the SARS-CoV-2 viral life cycle, we investigated the effects of EWSR1 silencing on transcription and translation of NP. First, we designed 3 short hairpin RNAs targeting the 5′ untranslated region , 3′ untranslated region, and the coding sequence (CDS) of EWSR1. Lentivirus was packaged to transduce Huh7 cells endogenously expressing ACE2. Knockdown efficiency was confirmed us-

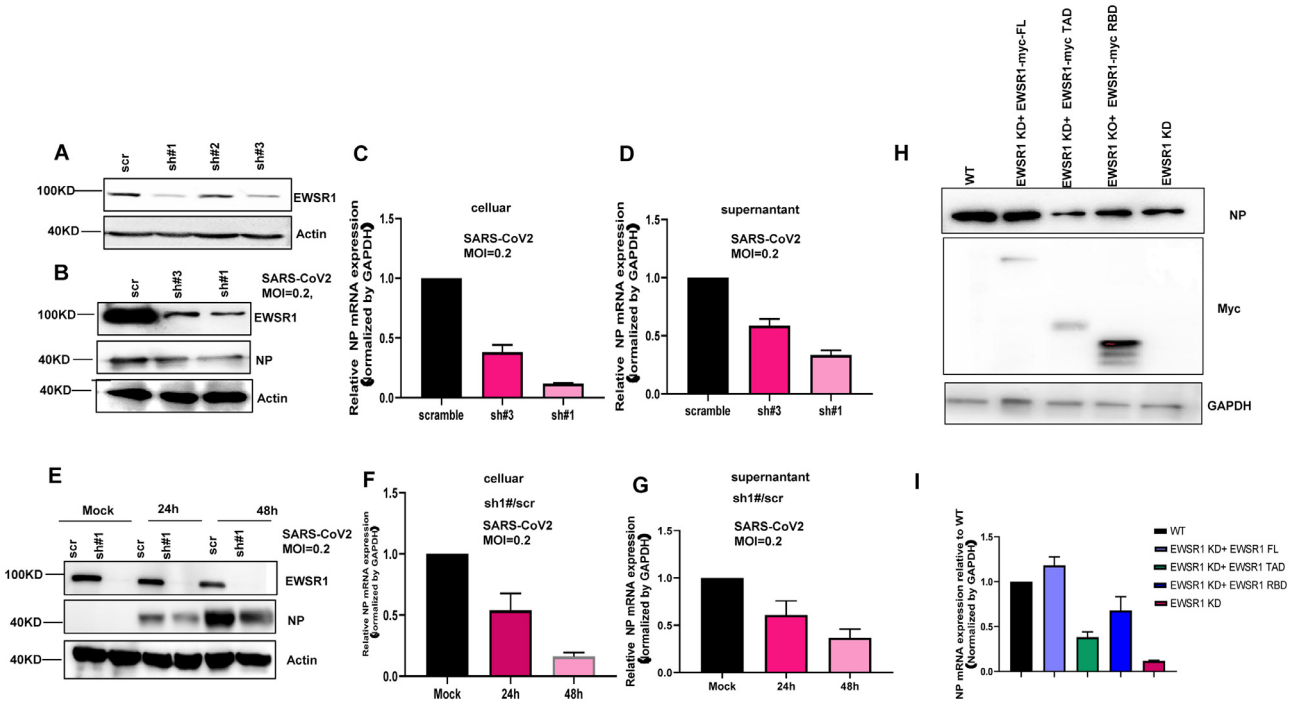

Fig. 4. EWSR1 is essential for SARS-CoV-2 replication. (A) Huh7 cells were infected twice with three shRNA-encoding lentiviruses and scrambled lentivirus. After puromycin selection, cells were harvested and lysed for western blot analysis with the EWSR1 antibody. (B–D) Huh7 cells stably expressing effective shRNA-1 and shRNA-3 targeting EWSR1 were infected with SARS-CoV-2 (MOI=0.2) for 48 h. At 48 h, cellular protein (B), cellular RNA (C), and viral RNA in the supernatant (D) were harvested. Cellular proteins were separated and analyzed by SDS-PAGE and immunoblotted for viral NP or actin. The NP mRNA was quantified using RT-qPCR, with results normalized to GAPDH gene expression. (E–G) Huh7 cells stably expressing effective shRNA-1 were infected with SARS-CoV-2 (MOI=0.2) for a time course of 24 h and 48 h. Cellular protein (E), cellular RNA (F), and viral RNA in the supernatant (G) were harvested. Cellular proteins were separated and analyzed by SDS-PAGE and immunoblotted for viral NP or actin. NP mRNA was quantified using RT-qPCR, normalized to GAPDH gene expression. (H–I) Huh7 cells stably expressing effective shRNA-1 were transduced with distinct myc-tagged EWSR1 truncations and then subjected to SARS-CoV-2 infection (MOI = 0.2) for 48 h. Cellular protein (H) or mRNA (I) was harvested. Cellular proteins were separated and analyzed by SDS-PAGE and immunoblotted for viral NP, actin or myc (indicated for respective EWSR1 truncation expression). NP mRNA was quantified using RT-qPCR, normalized to GAPDH gene expression.

ing an anti-EWSR1 antibody. Compared with an irrelevant scramble, shRNA-1 and shRNA-3 targeting ESWR1 resulted in a dramatic reduction of endogenous EWSR1 protein, indicating effective silencing (Fig. 4A). We then chose shRNA-1 and shRNA-3 for further SARS-CoV-2 virus infection experiments. We found that viral NP expression in EWSR1-silenced cells was significantly decreased compared with that in wild-type controls at 48 h postinfection (Fig. 4B). We also observed that NP mRNA expression in EWSR1-silenced cells as well as that in the supernatant were dramatically decreased compared with that in wild-type controls (Fig. 4C and D). Furthermore, we noticed a time-dependent decrease in NP levels (Fig. 4E) and mRNA expression both in cells and the supernatant (Fig. 4F and G) when using shRNA-1 in a time course of virus infection. These results suggest that silencing EWSR1 could inhibit virus propagation.

To rule out off-target effects of shRNA and identify which domain of EWSR1 promotes viral replication, we next determined whether SARS-CoV-2 replication could be restored by expression of full-length, TAD, or RBD domains of EWSR1. We therefore transduced EWSR1-silenced Huh7 cells with lentivirus encoding full length, TAD, or RBD EWSR1 and infected the cells with SARS-CoV-2. We found that NP (Fig. 4H) and NP mRNA levels (Fig. 4I) were restored in full-length EWSR1-transduced cells. Overexpression of EWSR1 RBD partially but not fully rescued the phenotype. Overexpression of TAD could not rescue NP expression, suggesting that the RBD of EWSR1 was essential for binding to NSP13 and enhancing its activity, thus promoting dsRNA unwinding and virus replication.

3.4. Purified recombinant EWSR1 promotes NSP13 helicase activity in vitro

Finally, we sought to examine whether EWSR1 binds to NSP13 and enhances its RNA helix unwinding activity. We expressed and purified His-tagged NSP13 and EWSR1 FL/TAD/RBD protein in a BL21-DE3 expression system (Fig. 5A). We also performed western blotting to confirm protein expression (Fig. S1A and 1B and 1C). We then constructed an RNA helix substrate with 5 protrusions by annealing a 42-nucleotide HEX-labeled RNA with a 24-nucleotide unlabeled RNA. This dsRNA helix was used to measure the helix unwinding efficiency of RNA helicases as reported by others [19]. The unwinding assay was performed by incubating the RNA helix substrate with NSP13

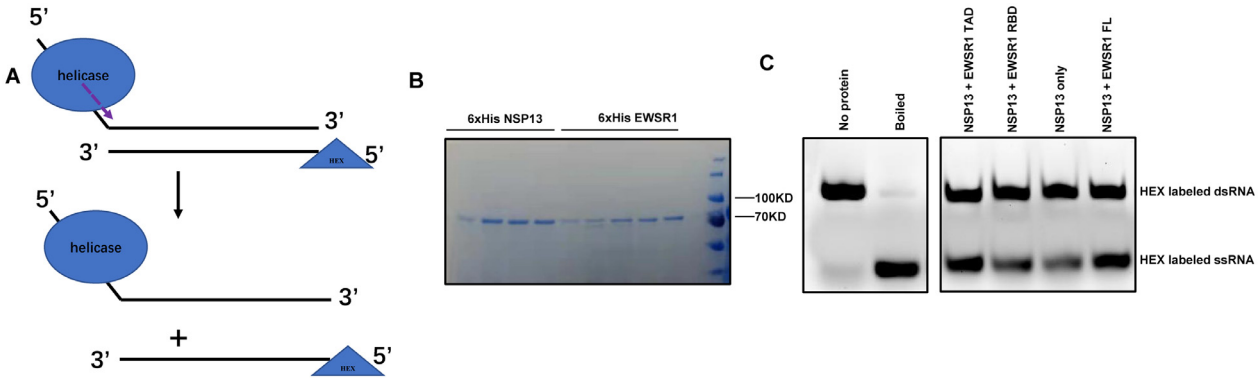

Fig. 5. Purified recombinant EWSR1 promotes the helicase activity of NSP13 in-vitro. (A) Schematic illustration of RNA helix substrate unwinding by SARS-CoV-2 helicase NSP13. (B) Expression and purification of His-tagged SARS-CoV-2 NSP13 and EWSR1 protein. Different amounts of protein were loaded into the gel wells and subjected to 10% SDS-PAGE, followed by Coomassie brilliant blue staining. (C) The RNA helix unwinding assay was performed in the presence of NSP13 only, or NSP13 with EWSR1 FL/TAD/RBD. dsRNA without any protein was the negative control and boiled dsRNA substrates were used as the positive control.

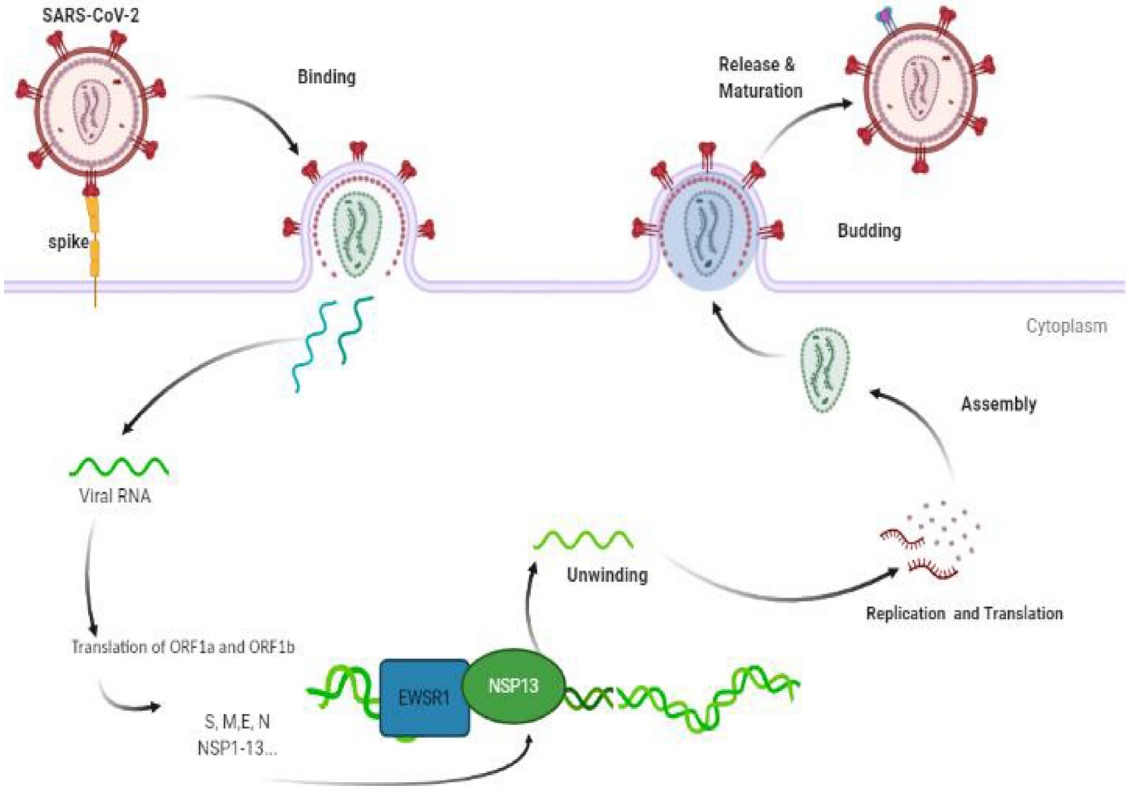

Fig. 6. The working model demonstrating the association of EWSR1 with NSP13 and promotion of SARA-CoV-2 unwinding and replication.

or other proteins of interest in a standard reaction mix containing $Mg^{2+}$and ATP, followed by separation of the RNA strands by RNA electrophoresis. dsRNA without any protein was the negative control and boiled dsRNA substrates were used as the positive control. The HEX-labeled RNA strand was released from the RNA helix substrate in the presence of NSP13 protein and either full-length EWSR1 or the RBD fragment, dramatically increasing the unwinding efficiency, but not in the presence of TAD (Fig. 5B), suggesting that EWSR1 promoted the unwinding activity of NSP13 by potentially binding to its NTPase domain in vitro. The RBD of ESWR1 is the critical binding domain for the interaction with NSP13 in vitro.

4. Discussion

By taking an unbiased approach to identifying host proteins that associate with SARS-CoV-2 helicase NSP13, we have for the first time defined EWSR1 as a host factor that shows enhancement of NSP13-mediated dsRNA unwinding. We also revealed that the RBD domain of EWSR1 specifically interacts with the NTPase domain of NSP13

and may enhance its unwinding activity. This binding was also confirmed by the in vitro dsRNA unwinding assay. We further employed loss of function approaches in SARS-CoV-2 infection to demonstrate that EWSR1 could promote viral replication and translation by physically binding to NSP13.

NSP13 facilitates virus replication by unwinding viral RNA, followed by RNA-dependent RNA polymerase (RdRP)-mediated replication and transcription of the SARS-CoV-2 genome, rendering NSP13 an advantageous target for drug development. NSP13 shows highest homology with the SARS-CoV helicase NSP13, suggesting the possible application of SARS-CoV NSP13 inhibitors in the context of SARS-CoV-2 infection. As expected, the 3 inhibitors of SARS-CoV NSP13 also displayed effective inhibition of SARS-CoV-2 virus infection.

Although a critical process, little is known about interactions between SARS-CoV-2 NSP13 and host proteins compared with other NSPs. Recently, affinity-purification mass spectrometry results have revealed that the NSP13 interactome contains proteins associated with organization of the centrosome and golgi, which may facilitate the rearrangement of the endoplasmic reticulum (ER) and golgi trafficking during coronavirus infection, especially in SARS-CoV-2 infection [39]. Furthermore, proximity-dependent biotinylation with the fast-acting mini turbo enzyme also confirmed that NSP13-associated proteins were ribosomal components that localized in the ER [40]. However, until now, there have been no functional experiments performed to investigate the specific proteins associated with SARS-CoV-2 NSP13 and their role in SARS-CoV-2 infection.

Here, we uncovered a previously uncharacterized interaction between NSP13 and host mRNA binding protein EWSR1. This interaction was shown by mass spectrometry and confirmed by co-immunoprecipitation assay. EWSR1 was first discovered as one of the chromosomal translocations that drives the majority of childhood and adolescent Ewing Sarcoma (EWS) cases. While its function in tumorigenesis is well established, little is known about its role during virus infection. A recent study reported that EWSR1 could directly bind to the hepatitis C virus genome, promoting efficient viral replication. EWSR1 was also reported to directly bind to the pan-viral genome as a host factor. It would be intriguing to elucidate whether EWSR1 and NSP13 binds on the same sites/regions of the SARS-CoV-2 RNA genomes or they binds the SARS-CoV-2 RNA genomes in a proximal distance, thus providing a spatial advantage for viral replication. Further studies will be needed to address this question.

The interaction between virus and host is an evolutionarily mutual interaction; the virus needs a variety of host resources and materials to establish and maintain an effective and persistent infection. We have demonstrated that SARS-CoV-2 NSP13 binds to EWSR1 and may hijack this host factor for building its own replication factory, but further studies are required to address how EWSR1 is recruited and binds to NSP13 during SARS-CoV-2 infection. Furthermore, rational design of small inhibitors to prevent this binding process may represent a promising strategy for drug development Fig. 6.

Declaration of competing interest

The authors declare that they have no known competing financial interests or personal relationships that could have appeared to influence the work reported in this paper.

Acknowledgement

We thank Prof. Pei-hui Wang from Shandong University for kindly providing us with the NSP13 plasmids.

Author contributions

ZZ, HZ, and GX conceived and designed the experiments. HZ, XG, GX, SZ, LC, and TX performed the experiments. WZ analyzed the data. ZZ and GX supervised the study. ZZ, HZ, and GX wrote the manuscript with input from all other authors. All authors discussed the data and approved the submission.

Funding

This work was supported by grants from the National Science Fund for Distinguished Young Scholars (82025022), the Central Charity Fund of Chinese Academy of Medical Science (2020-PT310–009), the Science and Technology Innovation Committee of Shenzhen Municipality (2020A1111350032) and the China Postdoctoral Science Foundation (2021M693359).

Supplementary materials

Supplementary material associated with this article can be found, in the online version, at doi:10.1016/j.imj.2021.12.004.

References

[1] N. Zhu, D. Zhang, W. Wang, et al., A Novel Coronavirus from Patients with Pneumonia in China, 2019, The New England journal of medicine 382 (2020) 727–733.
[2] D. Wang, B. Hu, C. Hu, et al., Jama, Clinical Characteristics of 138 Hospitalized Patients With 2019 Novel Coronavirus-Infected Pneumonia in Wuhan, China 323 (2020) 1061–1069.
[3] Z.Y. Zu, M.D. Jiang, P.P. Xu, et al., Coronavirus Disease 2019 (COVID-19): A Perspective from China, Radiology 296 (2020) E15–e25.
[4] (2020) [The epidemiological characteristics of an outbreak of 2019 novel coronavirus diseases (COVID-19) in China], Zhonghua liu xing bing xue za zhi = Zhonghua liuxingbingxue zazhi. 41, 145–151.
[5] J.F. Chan, S. Yuan, K.H. Kok, et al., A familial cluster of pneumonia associated with the 2019 novel coronavirus indicating person-to-person transmission: a study of a family cluster, Lancet 395 (2020) 514–523.
[6] J. Cui, F. Li, Z.L. Shi, Origin and evolution of pathogenic coronaviruses, Nature reviews Microbiol 17 (2019) 181–192.
[7] Y. Zhang, J. Zhang, Y. Chen, et al. (2020) The ORF8 Protein of SARS-CoV-2 Mediates Immune Evasion through Potently Downregulating MHC-I, bioRxiv: the preprint server for biology, 2020.05.24.111823.

[8] X. Lei, X. Dong, R. Ma, et al., Activation and evasion of type I interferon responses by SARS-CoV-2, Nat Commun 11 (2020) 3810.
[9] J.-.Y. Li, C.-.H. Liao, Q Wang, et al., The ORF6, ORF8 and nucleocapsid proteins of SARS-CoV-2 inhibit type I interferon signaling pathway, Virus Res. 286 (2020) 198074.
[10] L. Miorin, T. Kehrer, M.T. Sanchez-Aparicio, et al., SARS-CoV-2 Orf6 hijacks Nup98 to block STAT nuclear import and antagonize interferon signaling, Proc. National Acad Sci 117 (2020) 28344.
[11] Q. Peng, R. Peng, B. Yuan, et al., Structural and biochemical characterization of the nsp12-nsp7-nsp8 core polymerase complex from SARS-CoV-2, Cell Rep 31 (2020) 107774.
[12] D.G. Ahn, J.K. Choi, D.R. Taylor, J.W. Oh, Biochemical characterization of a recombinant SARS coronavirus nsp12 RNA-dependent RNA polymerase capable of copying viral RNA templates, Arch. Virol. 157 (2012) 2095–2104.
[13] Y. Gao, L. Yan, Y. Huang, et al., Structure of the RNA-dependent RNA polymerase from COVID-19 virus, Science (New York, NY) 368 (2020) 779–782.
[14] A.O. Adedeji, K. Singh, N.E. Calcaterra, et al., Severe acute respiratory syndrome coronavirus replication inhibitor that interferes with the nucleic acid unwinding of the viral helicase, Antimicrob. Agents Chemother. 56 (2012) 4718–4728.
[15] K.A. Ivanov, V. Thiel, J.C. Dobbe, Y. van der Meer, E.J. Snijder, J. Ziebuhr, Multiple enzymatic activities associated with severe acute respiratory syndrome coronavirus helicase, J. Virol. 78 (2004) 5619–5632.
[16] C. Lee, J.M. Lee, N.R. Lee, D.E. Kim, Y.J. Jeong, Y. Chong, Investigation of the pharmacophore space of Severe Acute Respiratory Syndrome coronavirus (SARS-CoV) NTPase/helicase by dihydroxychromone derivatives, Bioorg. Med. Chem. Lett. 19 (2009) 4538–4541.
[17] J.A. Tanner, R.M. Watt, Y.B. Chai, et al., The severe acute respiratory syndrome (SARS) coronavirus NTPase/helicase belongs to a distinct class of 5′ to 3′ viral helicases, J. Biol. Chem. 278 (2003) 39578–39582.
[18] S. Yuan, R. Wang, J.F.-W. Chan, et al., Metallodrug ranitidine bismuth citrate suppresses SARS-CoV-2 replication and relieves virus-associated pneumonia in Syrian hamsters, Nature Microbiol 5 (2020) 1439–1448.
[19] T. Shu, M. Huang, D. Wu, et al., SARS-Coronavirus-2 Nsp13 Possesses NTPase and RNA Helicase Activities That Can Be Inhibited by Bismuth Salts, Virol Sin 35 (2020) 321–329.
[20] F. Bleichert, S.J. Baserga, The long unwinding road of RNA helicases, Mol. Cell 27 (2007) 339–352.
[21] J. Yang, Z. Cheng, S. Zhang, et al., A cypovirus VP5 displays the RNA chaperone-like activity that destabilizes RNA helices and accelerates strand annealing, Nucleic Acids Res. 42 (2014) 2538–2554.
[22] E. Mastrangelo, M. Pezzullo, T. De Burghgraeve, et al., Ivermectin is a potent inhibitor of flavivirus replication specifically targeting NS3 helicase activity: new prospects for an old drug, J. Antimicrob. Chemother. 67 (2012) 1884–1894.
[23] T. Himaki, Y. Masui, K. Chono, et al., Efficacy of ASP2151, a helicase-primase inhibitor, against thymidine kinase-deficient herpes simplex virus type 2 infection in vitro and in vivo, Antiviral Res. 93 (2012) 301–304.
[24] M.A. White, W. Lin, X. Cheng, Discovery of COVID-19 Inhibitors Targeting the SARS-CoV-2 Nsp13 Helicase, The journal of physical chemistry letters 11 (2020) 9144–9151.
[25] P. He, J. Ding, EWS promotes cell proliferation and inhibits cell apoptosis by regulating miR-199a-5p/Sox2 axis in osteosarcoma, Biotechnol. Lett. 42 (2020) 1263–1274.
[26] M. Azuma, L.J. Embree, H. Sabaawy, D.D. Hickstein, Ewing sarcoma protein ewsr1 maintains mitotic integrity and proneural cell survival in the zebrafish embryo, PLoS ONE 2 (2007) e979.
[27] N. Araya, K. Hirota, Y. Shimamoto, et al., Cooperative interaction of EWS with CREB-binding protein selectively activates hepatocyte nuclear factor 4-mediated transcription, J. Biol. Chem. 278 (2003) 5427–5432.
[28] P. Aman, I. Panagopoulos, C. Lassen, et al., Expression patterns of the human sarcoma-associated genes FUS and EWS and the genomic structure of FUS, Genomics 37 (1996) 1–8.
[29] Y.-.L. Wang, H. Chen, Y.-.Q. Zhan, et al., EWSR1 regulates mitosis by dynamically influencing microtubule acetylation, Cell Cycle 15 (2016) 2202–2215.
[30] H. Zinszner, R. Albalat, D. Ron, A novel effector domain from the RNA-binding protein TLS or EWS is required for oncogenic transformation by CHOP, Genes Dev. 8 (1994) 2513–2526.
[31] T. Ohno, M. Ouchida, L. Lee, Z. Gatalica, V.N. Rao, E.S. Reddy, The EWS gene, involved in Ewing family of tumors, malignant melanoma of soft parts and desmoplastic small round cell tumors, codes for an RNA binding protein with novel regulatory domains, Oncogene 9 (1994) 3087–3097.
[32] Q. Li, A.L. Brass, A. Ng, Z. Hu, R.J. Xavier, T.J. Liang, S.J. Elledge, A genome-wide genetic screen for host factors required for hepatitis C virus propagation, Proc. Natl. Acad. Sci. U.S.A. 106 (2009) 16410–16415.
[33] R.A. Flynn, J.A. Belk, Y. Qi, et al. (2020) Systematic discovery and functional interrogation of SARS-CoV-2 viral RNA-host protein interactions during infection, bioRxiv: the preprint server for biology.
[34] M.S. Yu, J. Lee, J.M. Lee, et al., Identification of myricetin and scutellarein as novel chemical inhibitors of the SARS coronavirus helicase, nsP13, Bioorganic & medicinal chemistry letters 22 (2012) 4049–4054.
[35] N. Yang, J.A. Tanner, Z. Wang, et al., Inhibition of SARS coronavirus helicase by bismuth complexes, Chem Commun (Camb) (2007) 4413–4415.
[36] N. Yang, J.A. Tanner, B.J. Zheng, et al., Bismuth complexes inhibit the SARS coronavirus, Angew Chem Int Ed Engl 46 (2007) 6464–6468.
[37] N. Ticozzi, C. Vance, A.L. LeClerc, et al., Mutational analysis reveals the FUS homolog TAF15 as a candidate gene for familial amyotrophic lateral sclerosis, Am J of Med Genetics Part B: Neuropsychiatric Genetics 156 (2011) 285–290.
[38] Z. Jia, L. Yan, Z. Ren, et al., Delicate structural coordination of the Severe Acute Respiratory Syndrome coronavirus Nsp13 upon ATP hydrolysis, Nucleic Acids Res. 47 (2019) 6538–6550.
[39] D.E.Jang Gordon, G. M.Bouhaddou, J.Obernier M.Xu, et al., A SARS-CoV-2 protein interaction map reveals targets for drug repurposing, Nature 583 (2020) 459–468.
[40] P. Samavarchi-Tehrani, H. Abdouni, J.D.R. Knight, et al. (2020) A SARS-CoV-2 – host proximity interactome, bioRxiv: the preprint server for biology, 2020.09.03.282103.